Stability, elastic anisotropy, and electronic properties of Ca_2C_3*

Quan Zhang(张权)[1], Qun Wei(魏群)[2,†], Hai-Yan Yan(闫海燕)[3], Xuan-Min Zhu(朱轩民)[2], Jun-Qin Zhang(张军琴)[1], Xiao-Fei Jia(贾晓菲)[4], and Rong-Hui Yao(姚荣辉)[2]

[1] *School of Microelectronics, Xidian University, Xi'an* 710071, *China*
[2] *School of Physics and Optoelectronic Engineering, Xidian University, Xi'an* 710071, *China*
[3] *College of Chemistry and Chemical Engineering, Baoji University of Arts and Sciences, Baoji* 721013, *China*
[4] *Department of Electronic and Information Engineering, Ankang University, Ankang* 725000, *China*

(Received 4 January 2017; revised manuscript received 3 March 2017; published online 20 April 2017)

The systematic investigations of the mechanical, elastic, and electronic properties, and stability of the newly synthesized monoclinic $C2/m$-Ca_2C_3 are performed, based on the first-principles calculations. Ca_2C_3 is found to be mechanically and dynamically stable only from 0 GPa to 24 GPa. The elastic anisotropy studies show that Ca_2C_3 exhibits the elastic anisotropy increasing with the augment of pressure. Furthermore, using the HSE06 hybrid functional, the electronic properties of Ca_2C_3 under pressure are calculated. The structure can be regarded as a quasi-direct band gap semiconductor, and the pressure-induced direct-indirect band gap transition is studied in detail.

Keywords: carbides, first-principles calculations, elastic properties, electronic structure

PACS: 62.20.de, 62.20.dq, 71.20.–b **DOI:** 10.1088/1674-1056/26/6/066201

1. Introduction

The binary carbide consisting of metal or nonmetal, has various intriguing properties in physics and chemistry, and thus a large number of promising structures have been studied. The well-known nonmetal carbides, silicon carbides,[1–7] which are regarded as the third-generation semiconductor material, have been employed in the high temperature and voltage power devices and optical sensors, owing to the indirect wide band gap. Furthermore, the nano-SiC[2] also has obtained a wide application in superconductors and ceramics to enhance the critical current density or to utilize its refractory nature and low neutron absorption.[3–5] Recently, the superhard and superconductive boron carbide material (e.g. BC_3,[8,9] BC_5,[10,11] BC_7,[12,13] and B_2C,[14,15] etc.) have received increasing attention, and both experiments and computational simulations show that they are more thermally and chemically stable than pure diamond. In addition, a diversity of metal carbides, such as LiC_x,[16] TiC_x,[17,18] MgC_x,[19,20] and CaC_x[21–25] are reported. The spontaneous intercalation of cations in the two-dimensional Ti_3C_2 MXene layers, which was studied by Lukatskaya *et al.*,[17] provides a basis for the further study of the high volumetric capacitance. The magnesium methanide Mg_2C was first synthesized by Kurakevych *et al.*,[19] and the rare C^{4-}, which is observed, allows easy hydrolysis towards the alkaline-earth-metal carbide. Furthermore, the high pressure polymorph β-Mg_2C_3,[20] with the linear C_3^{4-} chains nearly aligned along the crystallographic c axis, was synthesized by Strobel *et al.* For the calcium carbides, the well-known CaC_6[21,22] and CaC_2[23] were also investigated widely to show an unexpected pressure-composition property, and even the pressure-induced superconductivity. All of these studies enrich the study of binary carbides, and provide guidance for applications. Recently, Li *et al.*[26] reported a series of novel stable and metastable calcium carbide phases (Ca_5C_2, Ca_2C, Ca_3C_2, CaC, and Ca_2C_3), and successfully synthesized the *Pnma*-Ca_2C and $C2/m$-Ca_2C_3 by using the in situ synchrotron powder x-ray diffraction measurements. In the present work, we systematically study the $C2/m$-Ca_2C_3 phase in the mechanical and dynamical stability, elastic anisotropy and electronic band structure and the partial density of states (PDOSs) under the action of pressure, to reveal the mechanical, elastic and electronic properties of Ca_2C_3.

2. Computational methods

All of the calculations are performed based on the first-principles calculations. The exchange and correlation functional is in the generalized gradient approximation (GGA) which is parameterized by Perdew, Burke, and Ernzerhof (PBE)[27] in the Cambridge Serial Total Energy Package (CASTEP) code,[28] and the density functional theory (DFT)[29,30] uses the Vanderbilt ultrasoft pseudopotentials.[31]

*Project supported by the National Natural Science Foundation of China (Grant Nos. 11204007 and 61474089), the Natural Science Basic Research Plan in Shaanxi Province, China (Grant Nos. 2016JM1026 and 2016JM1016), and the Natural Science Foundation from Education Committee of Shaanxi Province, China (Grant Nos. 16JK1049 and 16JK1016).

†Corresponding author. E-mail: weiaqun@163.com

© 2017 Chinese Physical Society and IOP Publishing Ltd

The Broyden–Fletcher–Goldfarb–Shanno (BFGS)[32] minimization scheme is used in geometry optimization, and the total energy convergence tests are within 1 meV/atom. For the $C2/m$-Ca_2C_3, the energy cutoff is 420 eV, and the k-point mesh is 11×9×9 in the Brillouin zone. The self-consistent convergence of the total energy is 5.0×10^{-6} eV/atom, the maximum ionic Hellmann–Feynman force is 0.01 eV/Å, the maximum stress is 0.02 GPa, and the maximum ionic displacement is 5.0×10^{-4} Å. Furthermore, the electronic properties are calculated by the Heyd–Scuseria–Ernzerhof (HSE06) hybrid functional.[33]

3. Results and discussion

As shown in Fig. 1, $C2/m$-Ca_2C_3 has two types of nonequivalent carbon atoms, i.e., 4*i* (0.04, 0, 0.2283) and 2*a* (0, 0, 0), and one type of calcium atom 4*i* (0.4017, 0, 0.7208). The Ca atoms are isolated cations, and the C atoms constitute a carbon trimer chain which is along the *c*-axis and has a length of 1.336-Å C–C bond at 0 GPa. The optimized lattice parameters at 0, 18.1, and 24 GPa are listed in Table 1. To make a comparison, the known values are also given. As can be seen, these values are in good agreement with each other at 18.1 GPa.

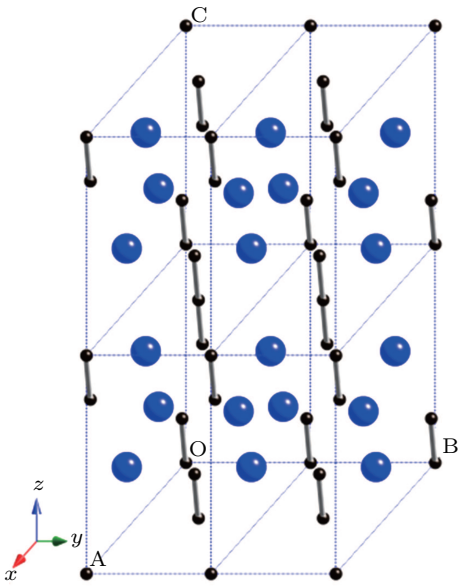


Fig. 1. (color online) 1×2×2 supercell of $C2/m$-Ca_2C_3. The black and blue spheres represent C and Ca atoms, respectively.

Table 1. Calculated lattice parameters, volume, and density.

		a/Å	*b*/Å	*c*/Å	*β* /(°)	*V*/(Å^3/atom)	*ρ* (g/cm^3)
Ca_2C_3	0 GPa	5.3909	5.3022	6.5661	128.4	14.72	2.622
	18.1 GPa	5.1441	4.9562	6.2979	128.81	12.51	3.084
		5.1511[26]	4.9620[26]	6.3059[26]	128.81[26]		
	24 GPa	5.0897	4.8829	6.2382	129.03	12.05	3.204

The plots of ratio X/X_0 as a function of pressure are presented in Fig. 2, and the degree of reducing along *b* axis is larger than those along the other two axes, indicating a lower anti-compressibility. Furthermore, since the C–C bond is along the *c* axis, Ca_2C_3 has the best ability to resist the compression along *c* axis.

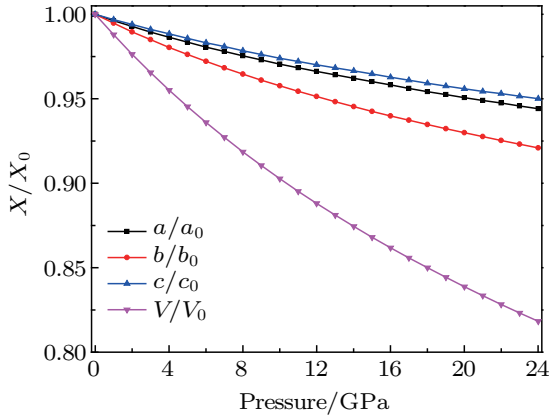


Fig. 2. (color online) Plots of the lattice parameter X/X_0 versus pressures.

To study the elastic property, the elastic constants and moduli of Ca_2C_3 are calculated and shown in Table 2. For the monoclinic phase, the generalized Born's mechanical stability criteria at 0 GPa are given as follows:[34,35]

$$C_{ii} > 0, i = 1, \ldots, 6, \tag{1}$$

$$[C_{11} + C_{22} + C_{33} + 2(C_{12} + C_{13} + C_{23})] > 0, \tag{2}$$

$$(C_{33}C_{55} - C_{35}^2) > 0, \tag{3}$$

$$(C_{44}C_{66} - C_{46}^2) > 0, \tag{4}$$

$$(C_{22} + C_{33} - 2C_{23}) > 0, \tag{5}$$

$$[C_{22}(C_{33}C_{55} - C_{35}^2) + 2C_{23}C_{25}C_{35} - C_{23}^2C_{55} - C_{25}^2C_{33}] > 0, \tag{6}$$

$$2[C_{15}C_{25}(C_{33}C_{12} - C_{13}C_{23}) + C_{15}C_{35}(C_{22}C_{13} - C_{12}C_{23}) + C_{25}C_{35}(C_{11}C_{23} - C_{12}C_{13})] - [C_{15}^2(C_{22}C_{33} - C_{23}^2) + C_{25}^2(C_{11}C_{33} - C_{13}^2) + C_{35}^2(C_{11}C_{22} - C_{12}^2)] + C_{55}g > 0, \tag{7}$$

$$g = C_{11}C_{22}C_{33} - C_{11}C_{23}^2 - C_{22}C_{13}^2 - C_{33}C_{12}^2 + 2C_{12}C_{13}C_{23}. \tag{8}$$

Based on the mechanical stability in crystal under isotropic pressure,[36] the mechanical stability criteria of the monoclinic phase at high pressure can be expressed as

$$\tilde{C}_{ii} > 0, \quad i = 1, \ldots, 6, \tag{9}$$

$$[\tilde{C}_{11}+\tilde{C}_{22}+\tilde{C}_{33}+2(\tilde{C}_{12}+\tilde{C}_{13}+\tilde{C}_{23})]>0, \quad (10)$$

$$(\tilde{C}_{33}\tilde{C}_{55}-C_{35}^2)>0, \quad (11)$$

$$(\tilde{C}_{44}\tilde{C}_{66}-C_{46}^2)>0, \quad (12)$$

$$(\tilde{C}_{22}+\tilde{C}_{33}-2\tilde{C}_{23})>0, \quad (13)$$

$$[\tilde{C}_{22}(\tilde{C}_{33}\tilde{C}_{55}-C_{35}^2)+2\tilde{C}_{23}C_{25}C_{35} -\tilde{C}_{23}^2\tilde{C}_{55}-C_{25}^2\tilde{C}_{33}]>0, \quad (14)$$

$$2[C_{15}C_{25}(\tilde{C}_{33}\tilde{C}_{12}-\tilde{C}_{13}\tilde{C}_{23})+C_{15}C_{35}(\tilde{C}_{22}\tilde{C}_{13}-\tilde{C}_{12}\tilde{C}_{23}) +C_{25}C_{35}(\tilde{C}_{11}\tilde{C}_{23}-\tilde{C}_{12}\tilde{C}_{13})] -[C_{15}^2(\tilde{C}_{22}\tilde{C}_{33}-\tilde{C}_{23}^2)+C_{25}^2(\tilde{C}_{11}\tilde{C}_{33}-\tilde{C}_{13}^2) +C_{35}^2(\tilde{C}_{11}\tilde{C}_{22}-\tilde{C}_{12}^2)]+\tilde{C}_{55}g>0, \quad (15)$$

$$g=\tilde{C}_{11}\tilde{C}_{22}\tilde{C}_{33}-\tilde{C}_{11}\tilde{C}_{23}^2-\tilde{C}_{22}\tilde{C}_{13}^2 -\tilde{C}_{33}\tilde{C}_{12}^2+2\tilde{C}_{12}\tilde{C}_{13}\tilde{C}_{23}, \quad (16)$$

where $\tilde{C}_{ii}=C_{ii}-P$, $i=1,\ldots,6$, $\tilde{C}_{12}=C_{12}+P$, $\tilde{C}_{13}=C_{13}+P$, $\tilde{C}_{23}=C_{23}+P$, and P is the isotropic pressure. That the calculated results satisfy the criteria indicates that the structure is mechanically stable.

Table 2. Calculated values of elastic constant C_{ij}, bulk modulus B, shear modulus G, Young's modulus E, Poisson's ratio ν, B/G ratio, and universal anisotropy index A^{U} at various pressures.

Pressure/GPa	Ca_2C_3			
	0	12	24	25
C_{11}	171	232	292	303
C_{22}	142	245	342	352
C_{33}	212	281	336	346
C_{44}	30	29	28	27
C_{55}	41	57	69	82
C_{66}	52	54	55	55
C_{12}	42	50	60	66
C_{13}	53	107	162	162
C_{23}	20	39	53	52
C_{15}	–8	–22	–27	–29
C_{25}	–5	–8	–7	–4
C_{35}	24	22	21	31
C_{46}	–9	–10	–11	–10
B	82	126	167	
G	48	58	64	
E	121	151	170	
ν	0.255	0.301	0.33	
B/G	1.72	2.18	2.61	
A^{U}	0.978	1.561	2.399	

As listed in Table 2, the structure satisfies the above criteria in a pressure range from ambient pressure to 24 GPa. At 25 GPa and higher pressures, the criteria in Eq. (12) cannot be satisfied. This demonstrates that Ca_2C_3 has the mechanical stability only at pressure up to 24 GPa (see Table 2). The elastic constants under pressure are also presented in Fig. 3. From Fig. 3 it follows that C_{11}, C_{33}, and C_{13}, have similar increased tendencies, and the tendency of C_{22} is sharper than the others, indicating that C_{22} is the most sensitive to the pressure effect in all of the elastic constants. The phonon spectra are calculated to ensure the dynamical stability of structure. As shown in Fig. 4, because of no imaginary frequency in the whole Brillouin zone, Ca_2C_3 is dynamically stable at pressure up to 24 GPa. With Voigt–Reuss–Hill approximation,[37–39] the bulk modulus B and shear modulus G are calculated, and the Young's modulus E and Poisson's ratio ν are given by[39,40] $E=9BG/(3B+G)$ and $\nu=(3B-2G)/[2(3B+G)]$. The calculated values of B, G, and E increase with pressure rising. According to Pugh,[41] the ratio of bulk to shear modulus shows the brittle and ductile nature. When the B/G of material is less than 1.75, it shows a brittle manner. Conversely, it shows a ductile manner. For Ca_2C_3, except the ratio of 1.72 at 0 GPa, other ratios are larger than 1.75, and make this material ductile. The universal elastic anisotropy index[42] is $A^{\mathrm{U}}=5G_{\mathrm{V}}/G_{\mathrm{R}}+B_{\mathrm{V}}/B_{\mathrm{R}}-6$, and the nonzero values in Table 2 suggest the elastic anisotropy. As can be seen from this table, these values are 0.978, 1.561, and 2.399 at 0, 12, and 24 GPa, respectively, indicating that the anisotropy increases with pressure rising.

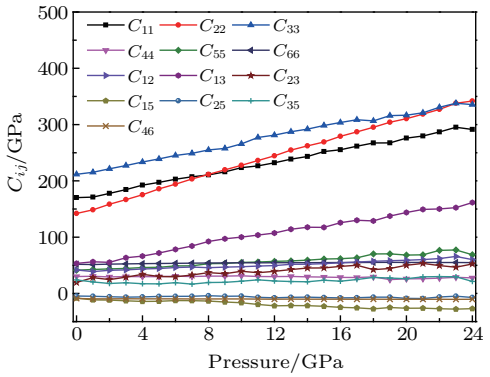


Fig. 3. (color online) Plots of elastic constant versus pressure.

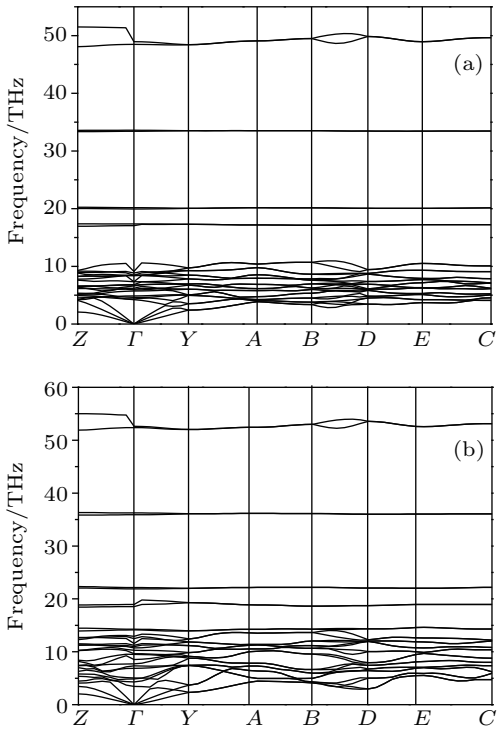


Fig. 4. Phonon spectra for $C2/m$-Ca_2C_3 at 0 GPa (a) and 24 GPa (b).

To study the elastic anisotropy in detail, the directional dependence of elastic anisotropy, calculated by the ElAM code,[43] is shown in Fig. 5. The solid and dashed lines represent the maximal and minimal positive values, respectively. The black, red and blue lines represent the *xy*, *xz*, and *yz* planes, respectively. In Figs. 5(a) and 5(b), the maxima of shear modulus at 0 GPa and 24 GPa are 77 GPa and 131 GPa, respectively, and the minima are 27 GPa and 24 GPa, respectively. As a result, the anisotropy of shear modulus increases with pressure rising, conforming to the results of the universal elastic anisotropy index. For each plane, the anisotropy in *yz* plane is the highest at both 0 GPa and 24 GPa, whereas the lowest is in *xy* plane at 0 GPa and in *xz* plane at 24 GPa. The Poisson's ratios of Ca_2C_3 in Figs. 5(c) and 5(d) have similar anisotropies at different pressures ($0.563/0.035 \approx 6.1$ at 0 GPa and $0.733/0.046 \approx 5.9$ at 24 GPa) and the lowest anisotropies at 0 GPa and 24 GPa are both in *xy* plane, respectively. The Poisson's ratios have the highest anisotropy in *yz* plane at 0 GPa, and in *xz* plane at 24 GPa, respectively.

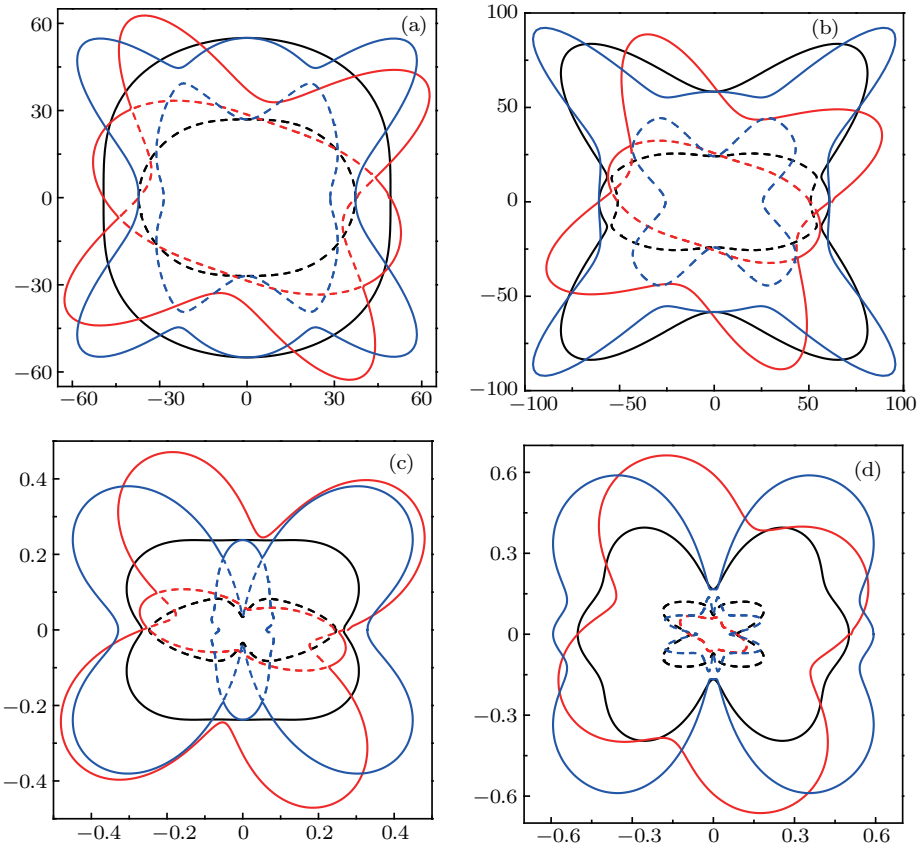


Fig. 5. (color online) 2D representations of shear modulus at 0 GPa (a) and at 24 GPa (b); and 2D representations of Poisson's ratio at 0 GPa (c) and at 24 GPa (d). The solid and dashed lines represent the maximal and minimal positive values, respectively. The black, red, and blue lines represent the projections in *xy*, *xz*, and *yz* planes, respectively.

The directional dependence of Young's modulus is shown in Figs. 6(a) and 6(b). A spherical shape indicates that the structure is isotropic. It is found that the anisotropy at 0 GPa is lower than that at 24 GPa, and the average Young's moduli in all directions are 125 GPa and 165 GPa, close to the 121 GPa and 170 GPa by Voigt–Reuss–Hill approximations, respectively. Figures 6(c) and 6(d) display the two-dimensional (2D) plots of differences in each direction of Young's modulus. The maxima at 0 GPa and 24 GPa are 211 GPa and 327 GPa, respectively, and the minima are 83 GPa and 87 GPa, respectively. The E_{max}/E_{min} ratios at 0 GPa and 24 GPa are 2.52 and 3.76, respectively. Furthermore, the highest anisotropies at 0 GPa and 24 GPa are in *xz* plane and *yz* plane, respectively, and the lowest anisotropies at 0 GPa and 24 GPa are in *xy* plane and *xz* plane, respectively.

The calculated electronic properties of Ca_2C_3 by the HSE06 functional are shown in Fig. 7. It is found that Ca_2C_3 is a semiconductor. At 0 GPa, the conduction band minimum (CBM) is located at Γ point and the valence band maximum (VBM) is at Z point with an indirect band gap of 1.81 eV (see Fig. 7(a)). At 3 GPa, both the CBM and the VBM are at Γ point with a direct band gap of 1.82 eV, which means that there occurs an indirect–direct band gap transition. At 24 GPa, the CBM is at Γ point, the VBM is at (−0.5, 0, 0.34) along the *B*–*D* direction. For convenience, we denote this point as *P* point. The indirect band gap is 1.63 eV. It is known that the GGA calculations usually underestimate the gap. As a result, our calculations by the HSE06 functional are larger than the available results at GGA level.[26]

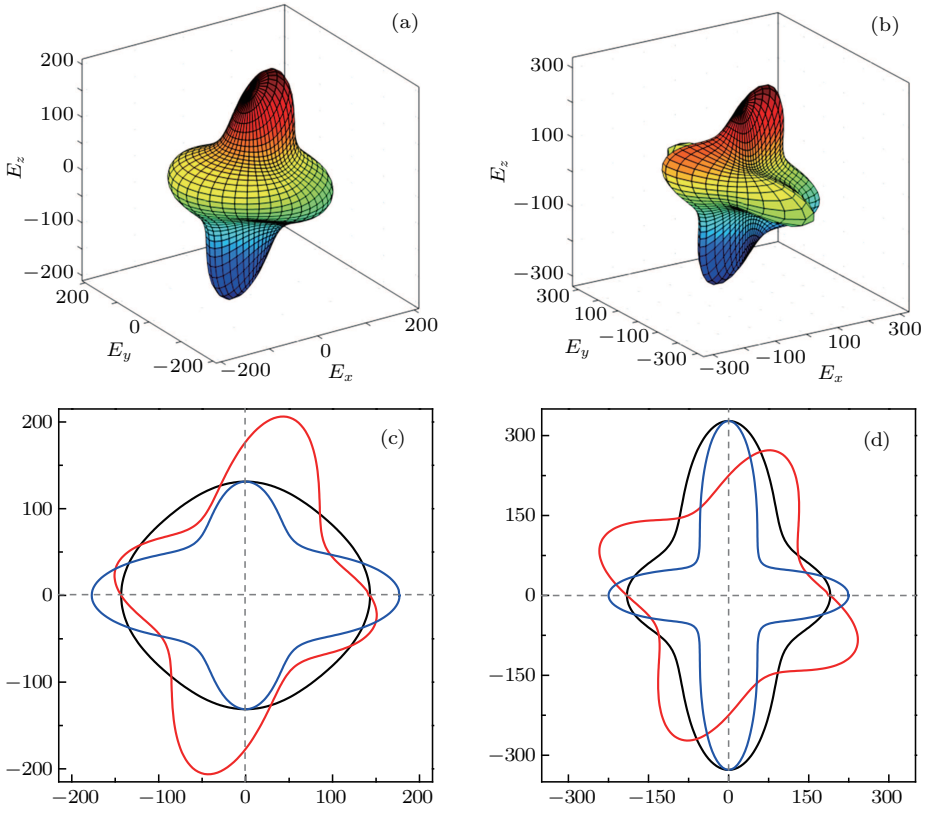


Fig. 6. (color online) Directional dependence of the Young's modulus at 0 GPa (a), and 24 GPa (b); and 2D representations of the Young's modulus at 0 GPa (c), and 24 GPa (d). The black, red, and blue lines represent the projections in *xy*, *xz*, and *yz* planes, respectively.

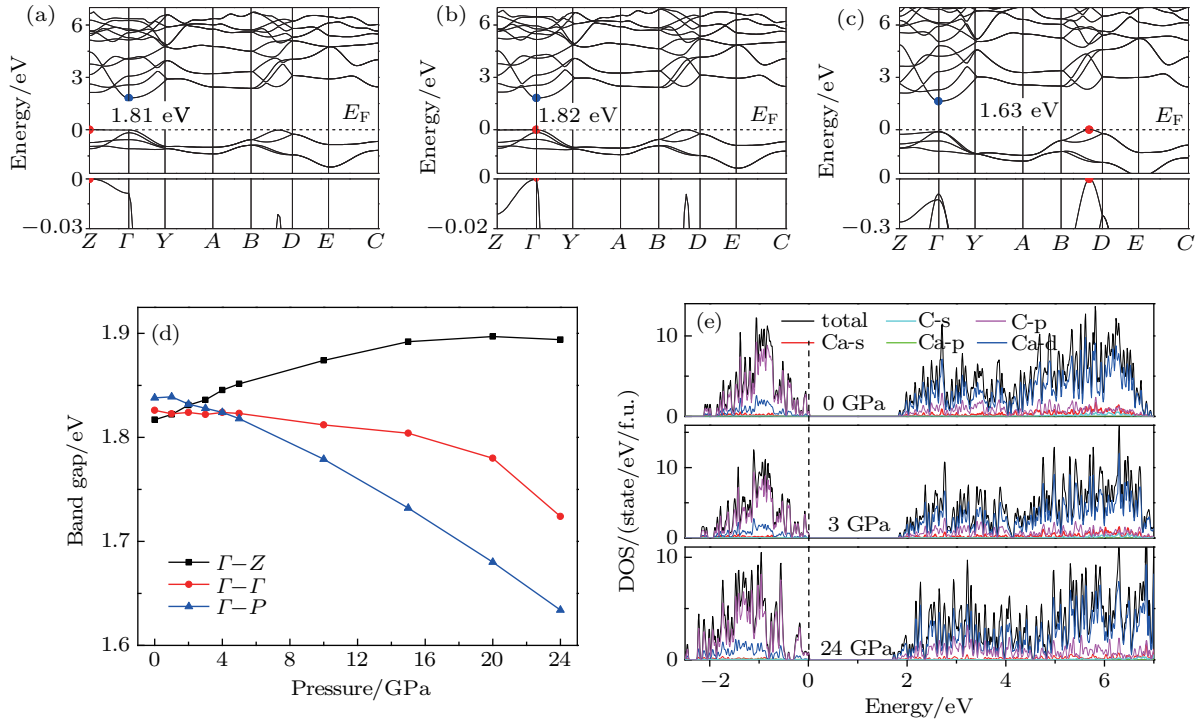


Fig. 7. (color online) Electronic band structures at 0 GPa (a), 3 GPa (b), and 24 GPa (c); the gaps of *Γ*–*Z*, *Γ*–*Γ*, and *Γ*–*P* each as a function of pressure (d); partial DOSs of Ca_2C_3 (e). The blue and red points represent CBM and VBM, respectively.

As seen in Figs. 7(a)–7(c), *Γ*, *Z*, and *P* points have almost the same energies. To clarify the energies of these three points, the magnifications near Fermi level are shown at the bottom of Figs. 7(a)–7(c). It can be seen that the difference between *Γ* and *Z* points is only about 0.01 eV, thus Ca_2C_3 is a quasi-direct band gap semiconductor. To show the indirect–direct–indirect transition in detail, the gaps of *Γ*–*Z*, *Γ*–*Γ*, and *Γ*–*P* under pressures are calculated, and the results are illustrated in Fig. 7(d). From this figure it follows that the transition points are about 1.1 GPa and 4.0 GPa, respectively. The

energy at Z point decreases with pressure increasing, however at P point it increases. For the Γ point, the energy increases below 4.0 GPa, whereas decreases from 4.0 GPa to 24.0 GPa. Figure 7(e) shows the total and partial DOS whose values decrease with pressure rising. The conduction band region is mainly characterized by the Ca-d states, and the valence band region is mainly contributed from the C-p states.

4. Conclusions

The mechanical, elastic, and electronic properties of Ca_2C_3 are investigated based on the first-principles calculations. We calculate the elastic constants and phonon spectra of Ca_2C_3, discovering that it has the mechanical and dynamical stability only in a pressure range from 0 GPa to 24 GPa, the instability at higher pressure is due to the mechanical instability. Furthermore, we find that this structure exhibits an increasing elastic anisotropy. As a semiconductor, the band gap of Ca_2C_3 can be regarded as quasi-direct at ambient pressure. The partial density of states is studied in detail, and the conduction band region is mainly characterized by the Ca-d states, and the valence band region is mainly contributed from the C-p states.

References

[1] Nakashima S and Harima H 1997 *Phys. Status Solidi A-Appl. Res.* **162** 39
[2] Dou S X, Soltanian S, Horvat J, Wang X L, Zhou S H, Ionescu M, Liu H K, Munroe P and Tomsic M 2002 *Appl. Phys. Lett.* **81** 3419
[3] Guo S Q, Yang J M, Tanaka H and Kagawa Y 2008 *Compos. Sci. Technol.* **68** 3033
[4] Lomello F, Bonnefont G, Leconte Y, Herlin-Boime N and Fantozzi G 2012 *J. Eur. Ceram. Soc.* **32** 633
[5] Wang R Z, Li W G, Li D Y and Fang D N 2015 *J. Eur. Ceram. Soc.* **35** 2957
[6] Pan F C, Chen Z P, Lin X L, Zheng F, Wang X M and Chen H M 2016 *Chin. Phys. B* **25** 096108
[7] Zhang Q, Wei Q, Yan H Y, Fan Q Y, Zhu X M, Zhang J Q and Zhang D Y 2016 *Z. Naturforsch. A* **71** 387
[8] Liu Z Y, He J L, Yang J, Guo X J, Sun H, Wang H T, Wu E D and Tian Y J 2006 *Phys. Rev. B* **73** 172101
[9] Liu H Y, Li Q, Zhu L and Ma Y M 2011 *Phys. Lett. A* **375** 771
[10] Solozhenko V L, Kurakevych O O, Andrault D, Le Godec Y and Mezouar M 2009 *Phys. Rev. Lett.* **102** 015506
[11] Li Q, Wang H, Tian Y J, Xia Y, Cui T, He J L, Ma Y M and Zou G T 2010 *J. Appl. Phys.* **108** 023507
[12] Xu L F, Zhao Z S, Wang Q Q, Wang L M, Xu B, He J L and Tian Y J 2011 *J. Appl. Phys.* **110** 013501
[13] Zhang Q, Wei Q, Yan H Y, Zhang Z X, Fan Q Y, Jia X F, Zhang J Q and Zhang D Y 2016 *Acta Phys. Pol. A* **129** 329
[14] Wang D Y, Yan Q, Wang B, Wang Y X, Yang J M and Yang G 2014 *J. Chem. Phys.* **140** 224704
[15] Fan Q Y, Wei Q, Chai C C, Yu X H, Liu Y, Zhou P K, Yan H Y and Zhang D Y 2015 *Chin. J. Phys.* **53** 100601
[16] Efthimiopoulos I, Benson D E, Konar S, Nylén J, Svensson G, Häussermann U, Liebig S, Ruschewitz U, Vazhenin G V, Loa I, Hanfl and Mand Syassen K 2015 *Phys. Rev. B* **92** 064111
[17] Lukatskaya M R, Mashtalir O, Ren C E, Dall'Agnese Y, Rozier P, Taberna P L, Naguib M, Simon P, Barsoum M W and Gogotsi Y 2013 *Science* **341** 1502
[18] Mashtalir O, Naguib M, Mochalin V N, Dall'Agnese Y, Heon M, Barsoum M W and Gogotsi Y 2013 *Nat. Commun.* **4** 1716
[19] Kurakevych O O, Strobel T A, Kim D Y and Cody G D 2013 *Angew. Chem. Engl.* **52** 8930
[20] Strobel T A, Kurakevych O O, Kim D Y, Godec Y L, Crichton W, Guignard J, Guignot N, Cody G D and Oganov A R 2014 *Inorg. Chem.* **53** 7020
[21] Debessai M, Hamlin J J, Schilling J S, Rosenmann D, Hinks D G and Claus H 2010 *Phys. Rev. B* **82** 132502
[22] Li Y L, Luo W, Chen X J, Zeng Z, Lin H Q and Ahuja R 2013 *Sci. Rep.* **3** 3331
[23] Nylen J, Konar S, Lazor P, Benson D and Haussermann U 2012 *J. Chem. Phys.* **137** 224507
[24] Nourbakhsh Z, Hashemifar S J and Akbarzadeh H 2013 *J. Alloys Compd.* **579** 360
[25] Wei Q, Zhang Q and Zhang M G 2016 *Materials* **9** 570
[26] Li Y L, Wang S N, Oganov A R, Gou H, Smith J S and Strobel T A 2015 *Nat. Commun.* **6** 6974
[27] Perdew J P, Burke K and Ernzerhof M 1996 *Phys. Rev. Lett.* **77** 3865
[28] Clark S J, Segall M D, Pickard C J, Hasnip P J, Probert M I J, Refson K and Payne M C 2005 *Z. Kristallogr.* **220** 567
[29] Hohenberg P and Kohn W 1964 *Phys. Rev.* **136** B864
[30] Kohn W and Sham L J 1965 *Phys. Rev.* **140** A1133
[31] Vanderbilt D 1990 *Phys. Rev. B* **41** 7892
[32] Pfrommer B G, Côté M, Louie S G and Cohen M L 1997 *J. Comput. Phys.* **131** 233
[33] Krukau A V, Vydrov O A, Izmaylov A F and Scuseria G E 2006 *J. Chem. Phys.* **125** 224106
[34] Wu Z J, Zhao E J, Xiang H P, Hao X F, Liu X J and Meng J 2007 *Phys. Rev. B* **76** 054115
[35] Xu X Y, Chai C C, Fan Q Y and Yang Y T 2017 *Chin. Phys. B* **26** 046101
[36] Sin'ko G V and Smirnov N A 2002 *J. Phys.: Condens. Matter* **14** 6989
[37] Voigt W 1928 *Lehrburch der Kristallphysik* (Leipzig, Germany: Teubner)
[38] Reuss A 1929 *Z. Angew. Math. Mech.* **9** 49
[39] Hill R 1952 *Phys. Soc. Lond. Sect. A* **65** 349
[40] Wei Q, Zhang Q, Yan H Y and Zhang M G 2017 *J. Mater. Sci.* **52** 2385
[41] Pugh S F 1954 *Lond. Edinb. Dublin Philos. Mag. J. Sci.* **45** 823
[42] Wei Q, Zhang M G, Yan H Y, Lin Z Z and Zhu X M 2014 *Europhys Lett.* **107** 27007
[43] Marmier A, Lethbridge Z A D, Walton R I, Smith C W, Parker S C and Evans K E 2010 *Comput. Phys. Commun.* **181** 2102